Supporting Information

Highly efficient and stable Ru nanoparticle electrocatalyst for the hydro-gen evolution reaction in alkaline conditions

Frederik Søndergaard-Pedersen,[a,b,†] Harish Lakhotiya,[a,b,†] Espen Drath Bøjesen,[b] Martin Bondesgaard,[a,b] Munkhshur Myekhlai,[c] Tania M. Benedetti,[c] J. Justin Gooding,[c,d] Richard D. Tilley,*[c,d,e] and Bo B. Iversen*[a,b]

[a]Center for Materials Crystallography, Department of Chemistry, Aarhus University, DK8000 Aarhus C (Denmark).[b]iNANO, Aarhus University, DK8000, Aarhus C (Denmark). [c]School of Chemistry, University of New South Wales, Sydney, New South Wales 2052 (Australia). [d]Electron Microscope Unit, Mark Wainwright Analytical Centre, University of New South Wales, Sydney, New South Wales 2052 (Australia). [e]Australian Research Council Centre of Excellence in Convergent Bio-Nano Science and Technology, University of New South Wales, Sydney, New South Wales 2052 (Australia)

Table of Contents

1. TEM images and particle size distribution

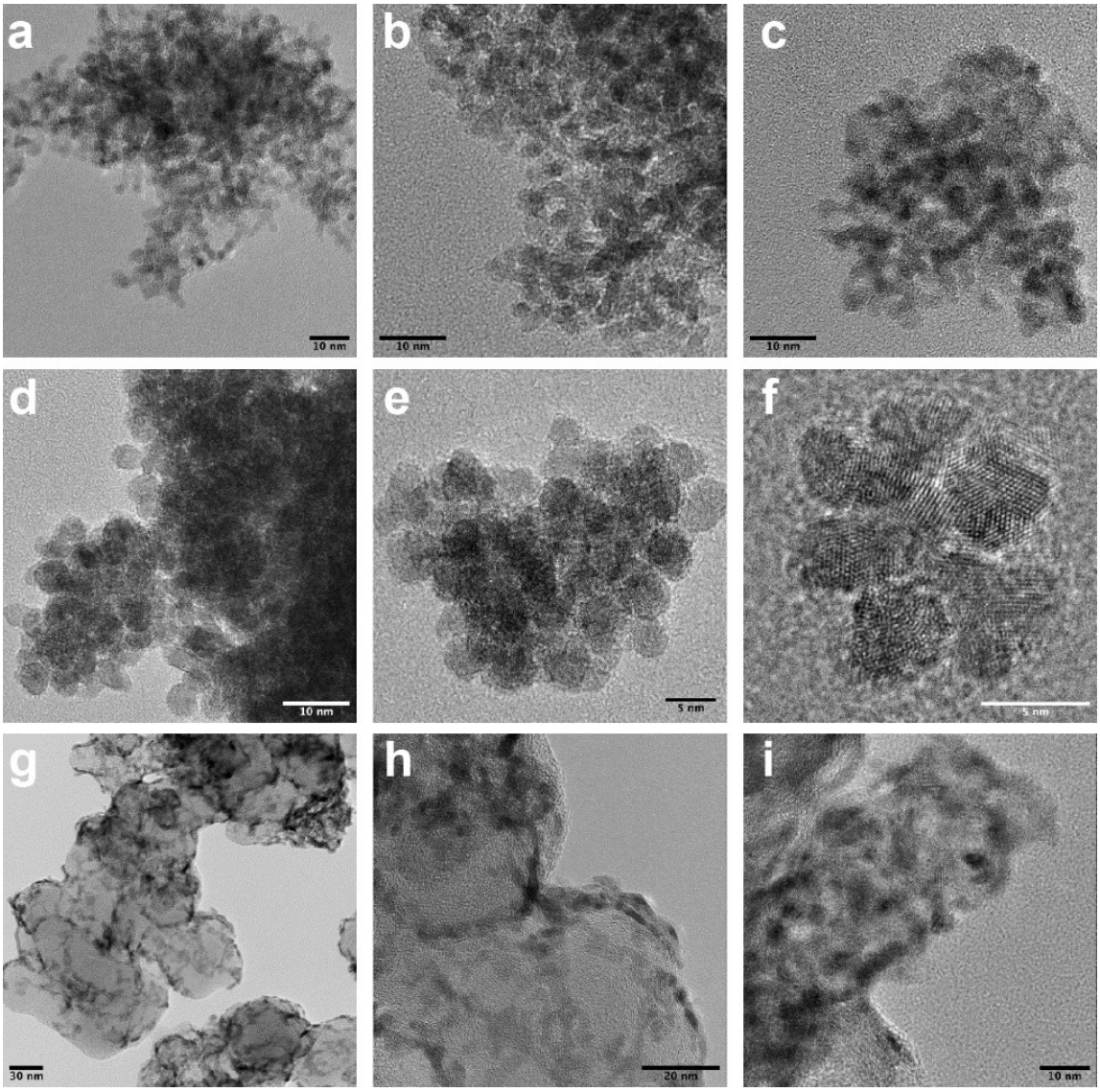

Figure S1. Additional TEM images of the Ru hcp (a,b,c), Ru fcc (d,e,f), and commercial Ru/C (g,h,i) samples showing quite monodisperse primary particles of a few nanometers in diameter that form agglomerates for both synthesized samples. The Ru/C sample shows much more anisotropic particle shapes and highlights the distribution of the particles across the carbon filler.

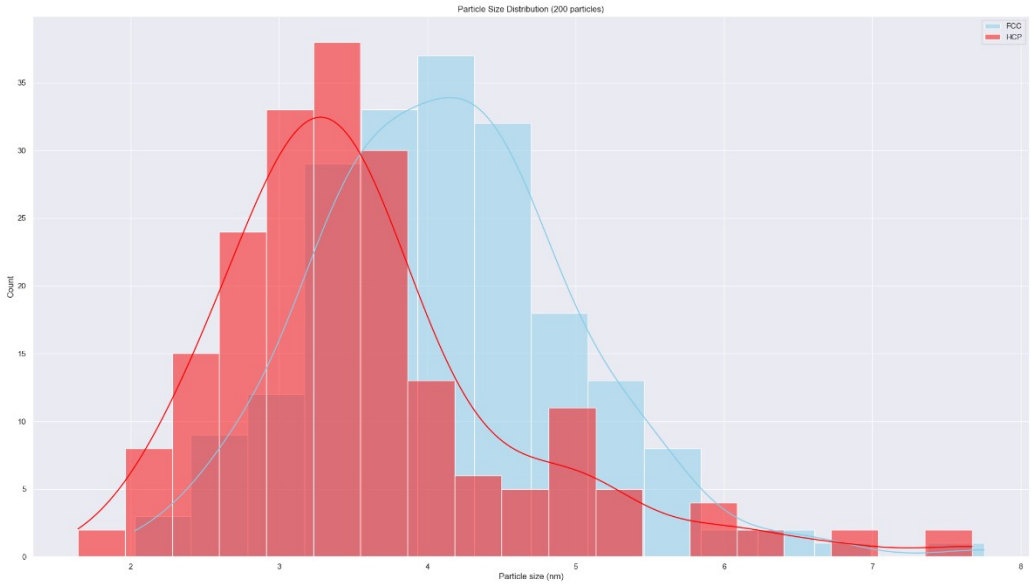

Figure S2. Average particle size distribution of the Ru fcc and Ru hcp samples.

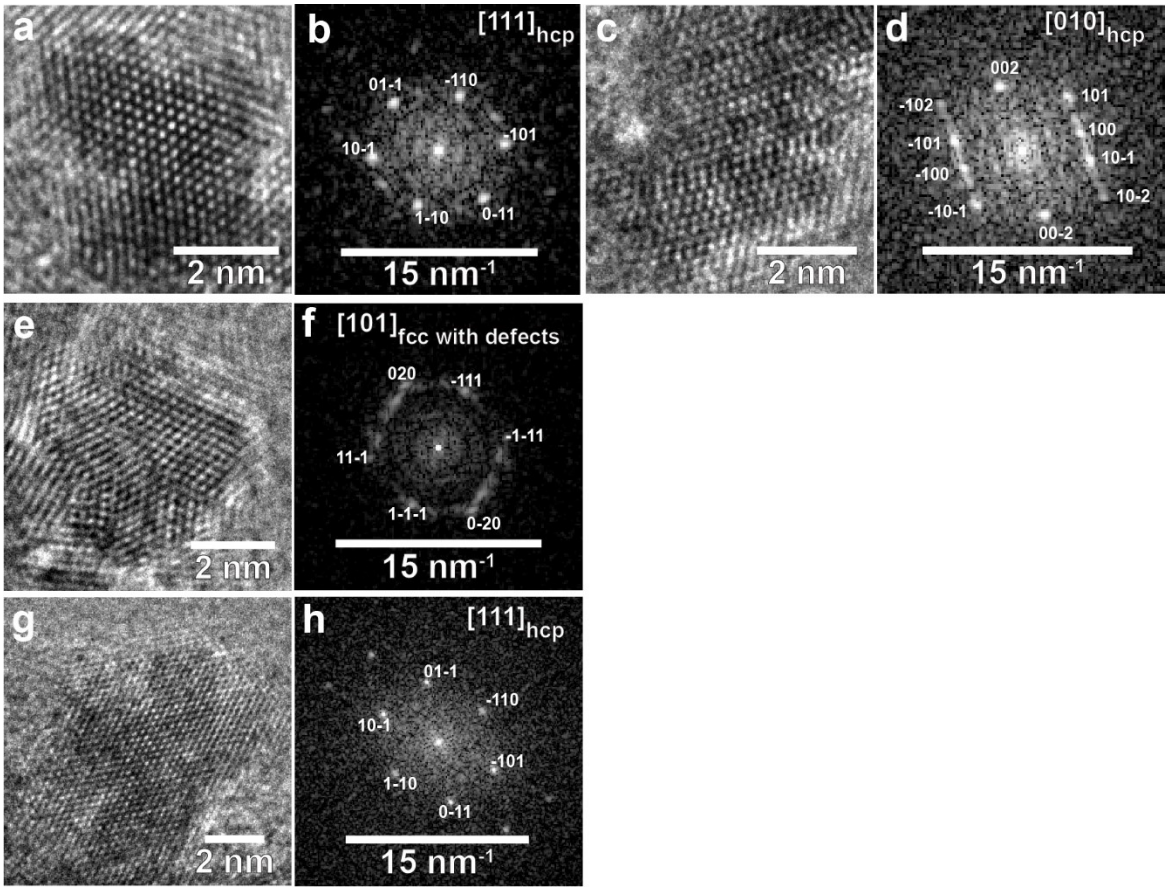

Figure S3. HR-TEM imaging and their respective FFTs indexed according to hcp for the Ru hcp sample (a,b,c,d), to fcc for the Ru fcc sample (e,f), and to hcp for the commercial Ru/C sample(g,h).

2. Rietveld refinements

Microstructural information about the samples was obtained by performing Rietveld refinements of the PXRD data in the FullProf suite using the Thompson-Cox-Hastings pseudo-Voigt formalism.[1] Instrumental peak broadening was taken into account by using an instrumental resolution file based on a measurement of a LaB_6 standard sample without any microstructural peak broadening. Anisotropic peak broadening was observed and this was modeled using the "Platelet Vector Size" model as implemented in FullProf with the close-packed directions defined as unique axes ([001] for the hcp sample and [111] for the fcc sample. This allowed extraction of crystallite sizes through refinement of the parameters Y and S_Z – average crystallite sizes are reported below. Furthermore, unit cell parameters were refined along with a scale factor and zero point correction. The background was modeled using linear interpolation between 3-4 manually selected point with refinable heights. Atomic B-values for Ru were fixed to 0.2.

Table S1. Parameters from Rietveld refinements

Sample	Ru hcp	Ru fcc
Space group	$P6_3/mmc$	Fm-3m
R_{Bragg}	3.22	4.69
R_F	2.57	3.55
a [Å]	2.7051(4)	3.955(1)
c [Å]	4.2994(6)	-
Y	1.568(8)	17.8(1)
S_Z	5.0(3)	-241(3)
Avg. crystallite size [nm]	3.3(2)	1.0(3)

3. STEM-EDS Elemental Mapping

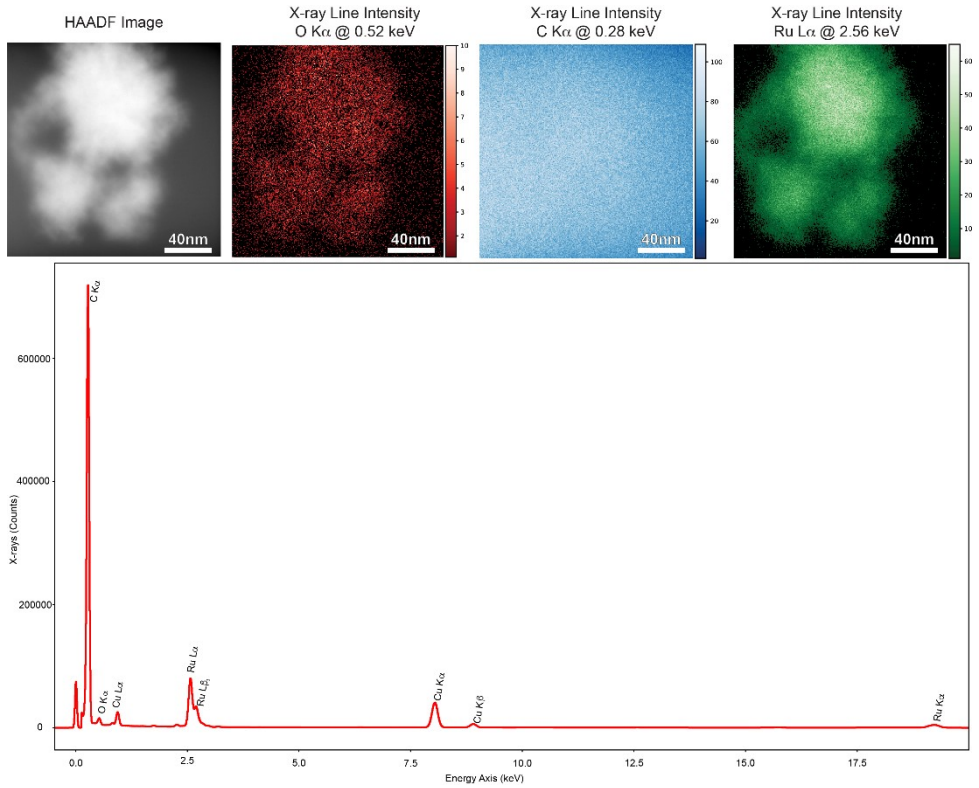

Figure S4. HAADF image and STEM-EDS elemental maps of the Ru hcp sample. STEM-EDS spectrum obtained for the Ru hcp sample with all major peaks indexed showing the presence of oxygen in addition to ruthenium. The additional peaks from Cu and C stem from the TEM grid.

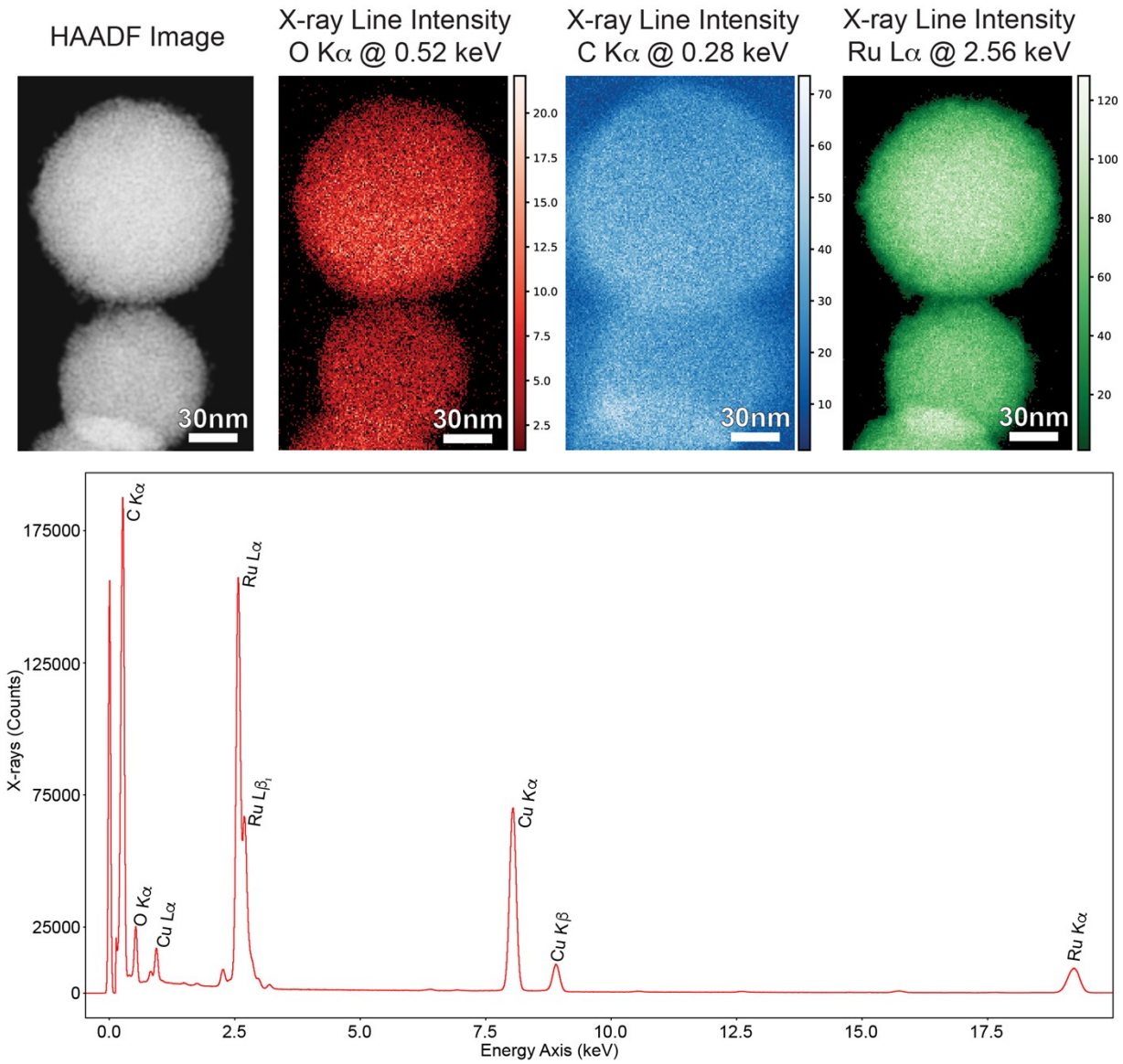

Figure S5 – HAADF image and STEM-EDS elemental maps of the Ru fcc sample. STEM-EDS spectrum with all major peaks indexed showing the presence of oxygen in addition to ruthenium. The additional peaks from Cu and C stem from the TEM grid.

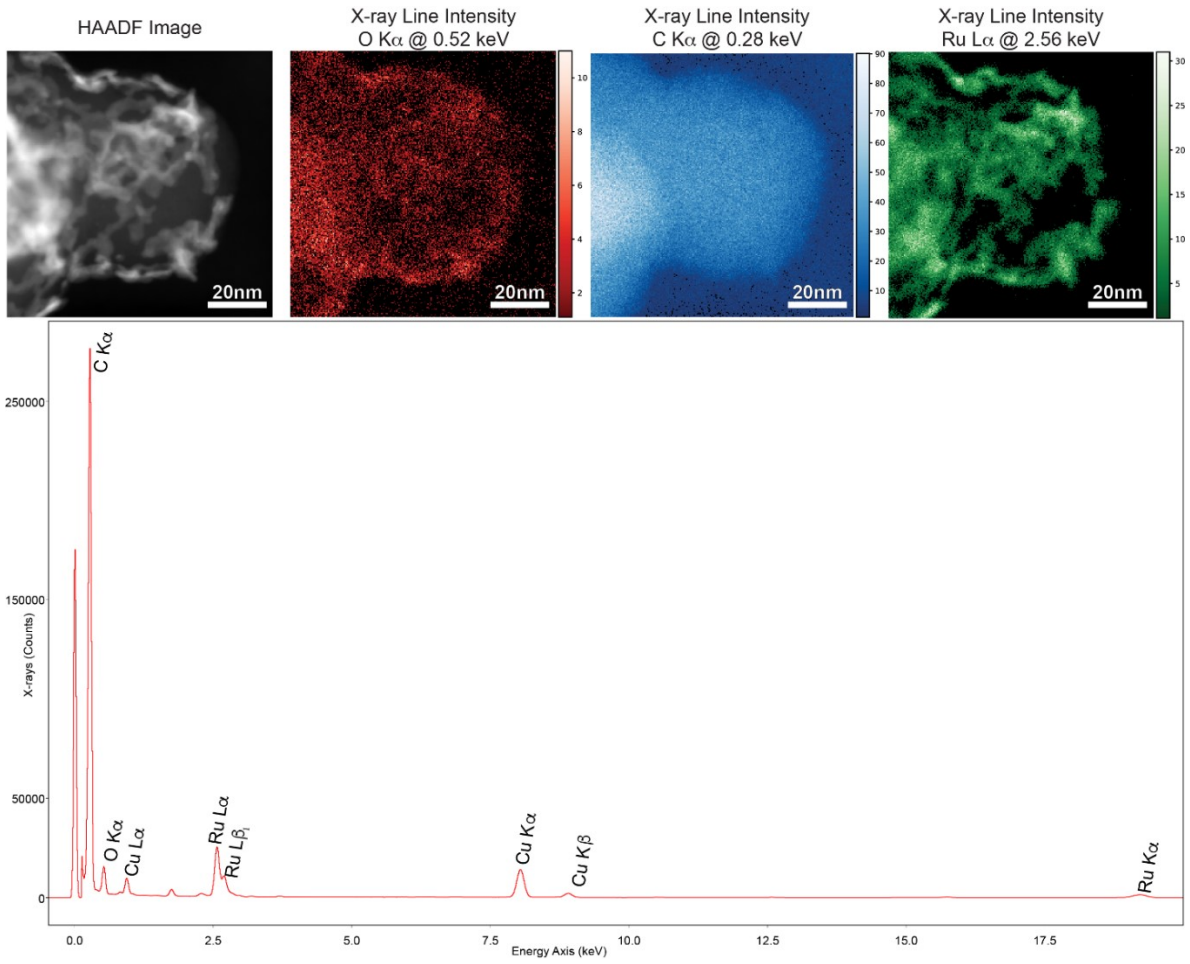

Figure S6. HAADF image and STEM-EDS elemental maps of the commercial Ru/C sample. STEM-EDS spectrum with all major peaks indexed showing the presence of oxygen in addition to ruthenium. The additional peaks from Cu and C stem from the TEM grid and C is also attributed to the Vulcan present in the sample.

4. XPS Spectra

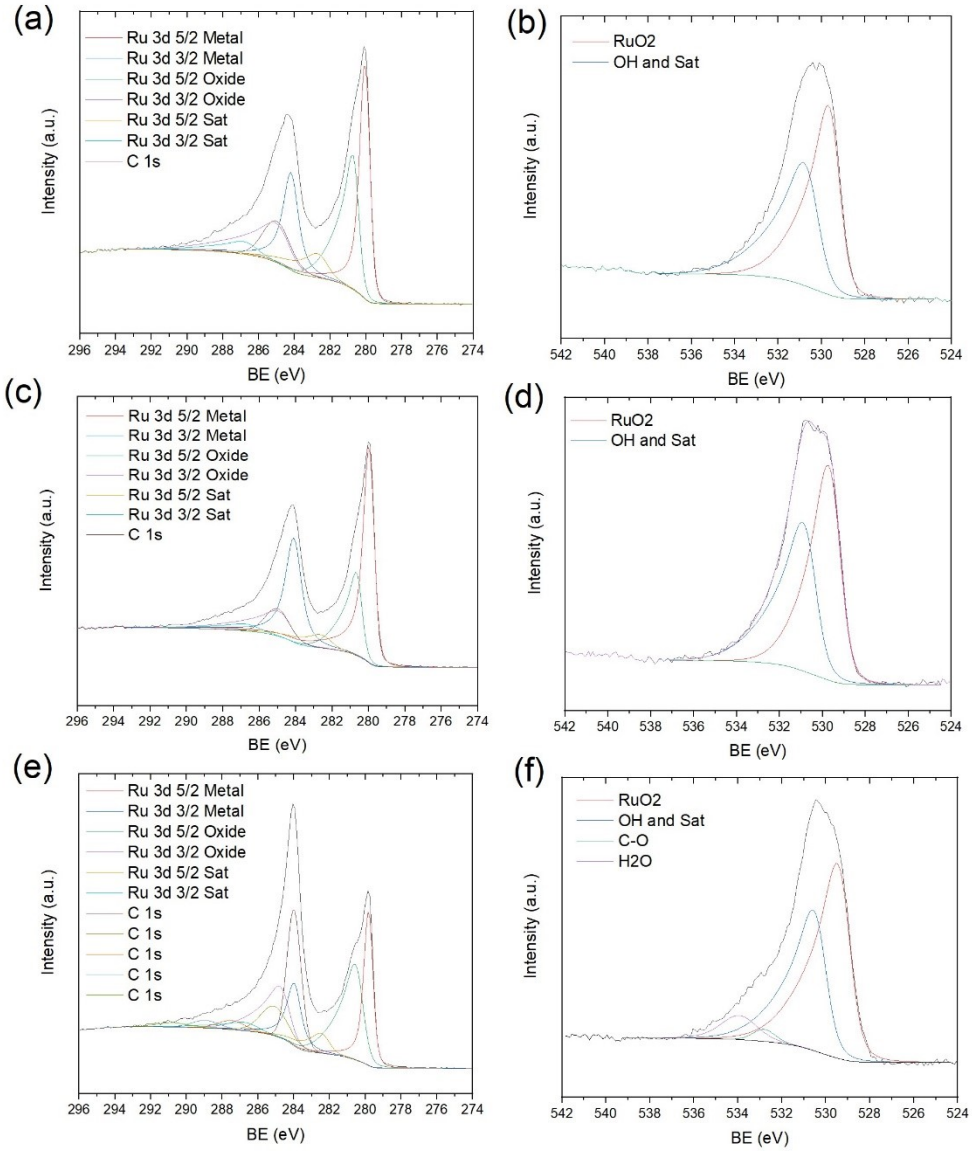

Figure S7. XPS of the Ru hcp (a,b), the Ru fcc (c,d) and the Ru/C (e,f) for C1s, Ru 3d and O 1s. Ru 3d peaks are distinguished further for 3/2 and 5/2 spin states.

5. TGA Analysis

The mass loss in the Ru fcc in the temperature interval 50 ˚C -180 ˚C is different from the Ru hcp. However, in general, the mass loss of the organic ligand is about 9.5% for both samples in the temperature range 50–600°C.

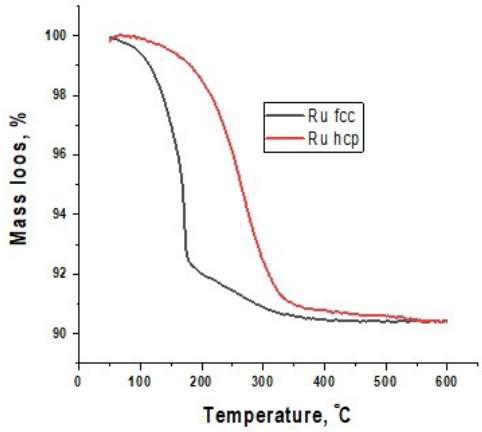

Figure S8. TGA of Ru-hcp and Ru-hcp

5. HER testing protocol

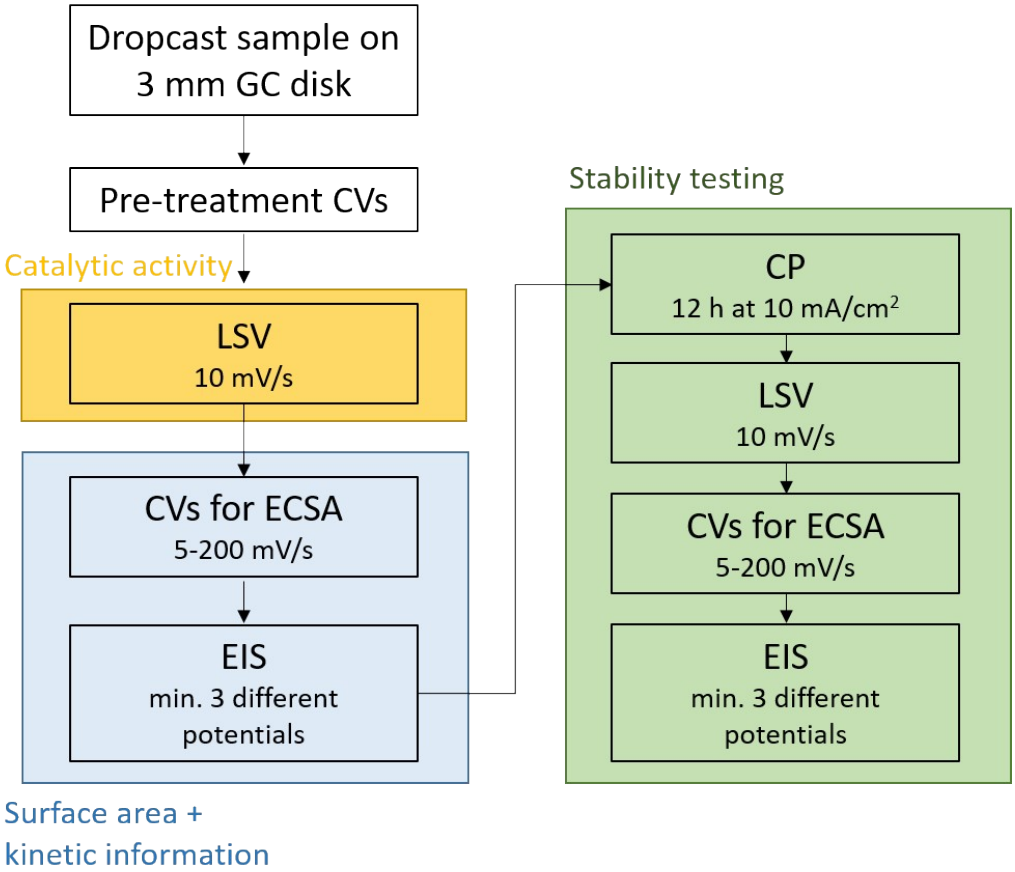

Figure S9. Testing protocol adopted for HER testing of all catalyst films deposited on glassy carbon (GC) rotating disk electrodes (RDE). The protocol consisted of linear sweep voltammetry (LSV), cyclic voltammetry (CV) for determination of electrochemically active surface areas (ECSAs), chronopotentiometry (CP) and electrochemical impedance spectroscopy (EIS).

6. Comparison of HER activity in alkaline conditions

Table S2. Comparison of most relevant Ru-based HER electrocatalysts in alkaline conditions.

Catalyst	Electrolyte	Size [nm]	η_{10} [mV]*	Tafel slope [mV/dec]	Reference
Ru hcp	1 M NaOH	3.3(2)	46	16 (CV) 21 (EIS)	This work
Ru fcc	1 M NaOH	1.0(3)	54	28 (CV) 38 (EIS)	This work
Comm. Ru/C	1 M NaOH	3(1)	51	27 (CV) 32(EIS)	This work
Comm. Pt/C	1 M NaOH	-	110	43 (CV)	This work
RuO_2-NWs@g-CN	0.5 M KOH	10-40 X 100-200	95	70	[2]
Ru@C_2N	1 M KOH	1.6	17	38	[3]
Hydrous RuO_2	1 M KOH	≈25	60	-	[4]
Crystalline RuO_2	1 M KOH	≈25	74	-	[4]
Ru-HPC	1 M KOH	2.87	≈5	33.9	[5]
PP-Ru/RuO_2-GC	1 M NaOH	1.5(3)	25	65	[6]
Ru/C	1 M KOH	1.73(47)	24	33	[7]
0.27-RuO_2@C	1 M KOH	5	20	46	[8]
Anhydrous-RuO_2@C	1 M KOH	150	63	62	[8]
fcc Ru/g-C_3N_4/C	0.1 M KOH	2	79	-	[9]
Ru fcc/hcp nanodendrites	1 M KOH	≈2	43.4	49	[10]

* Overpotential required to reach 10 mA/cm^2.

7. PXRD of Ru/C and Pt/C reference samples

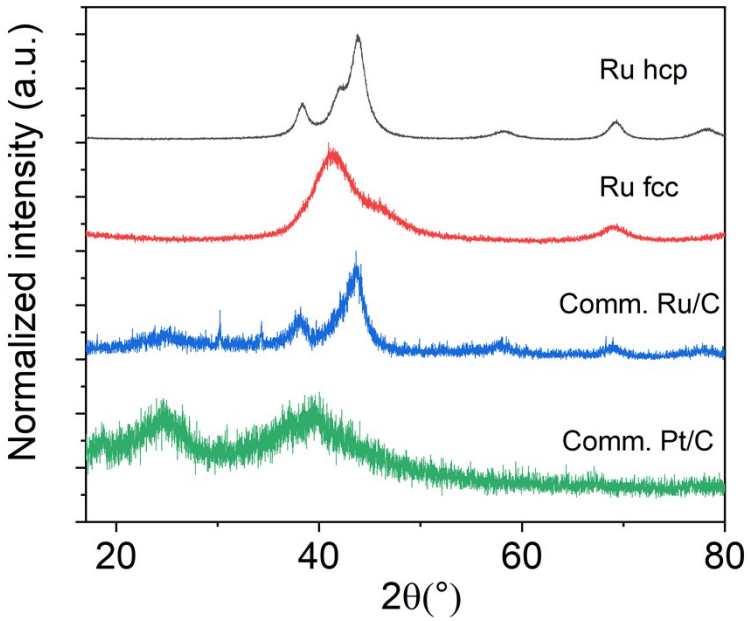

Figure S10. PXRD patterns of all tested samples including two commercial reference samples indicating that the commercial Ru/C sample contains nanoparticles with the hcp structure.

7. Modeling of EIS spectra

All the obtained EIS spectra display two slightly depressed semi-circles in the Nyquist plots. The high frequency semi-circles are nearly constant as a function of potential whereas the lower frequency semi-circles decrease in diameter as a function of increasing overpotential indicating that these represent the HER reaction (see Figure S13 for Ru hcp). The presence of two semi-circles can be due to incomplete coverage of the GC electrode by the catalyst film, the presence of an oxidized surface layer or even due to reduction of ruthenium oxide.

The EIS spectra could all be fitted using the model shown in Figure S14. This has previously been used to represent an electrode covered by an incomplete catalyst film (see fit results in table S4).[11] In this case, Q3 and R3 represent the interface between the catalyst film and the electrolyte. However, to take into account that the prepared films are not covering the electrode perfectly, Q1 and R2 represent the interface between the bulk GC electrode and the electrolyte. R1 represents the uncompensated resistance, which is used for performing iR-corrections of the data. The fitted values of R3 were interpreted as the charge transfer resistance, R_{ct}, as these displayed the expected behavior of decreasing R_{ct} with increasing overpotential for the HER reaction and they occurred in the expected frequency range of the EIS spectrum (the semi-circle at lower frequency) for electron transfers occurring as part of the HER reaction.[12] The fitted values of R2 were approximately constant as a function of potential.

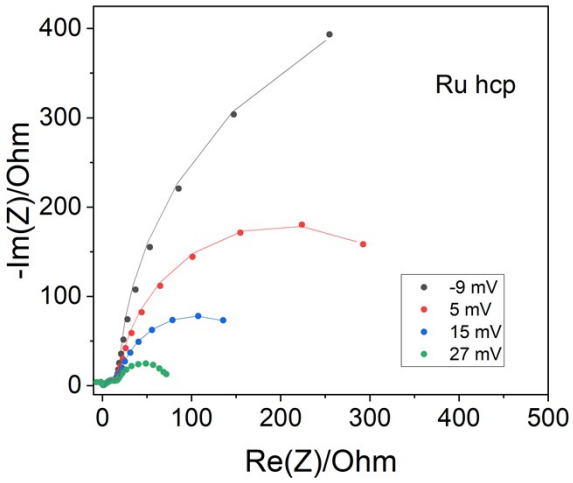

Figure S11. Nyquist plot of the obtained EIS spectra for the Ru hcp sample at varying overpotentials in the range -9 mV to 27 mV.

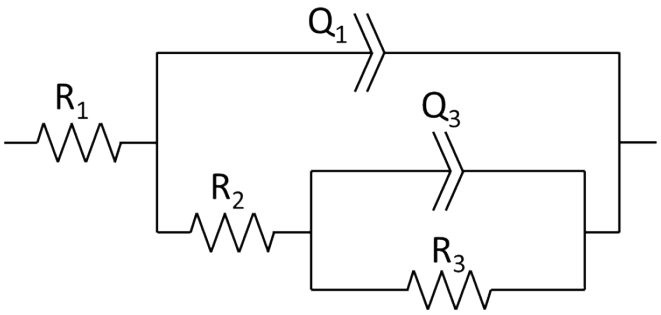

Figure S12. Equivalent circuit model used for fitting EIS data.

Table S3. Fitted parameters from equivalent circuit modeling of EIS spectra.

η (mV)	R1 (Ω)	Q1 (F s^{a-1})	a1	R2 (Ω)	Q3 (F s^{a-1})	a3	R3 (Ω)
Ru hcp new film							
-8.55	22.37	0.00124	0.875	18.71	0.0135	0.999	906.2
5.45	22.66	0.00105	0.862	18.75	0.0116	0.986	371.1
15.45	21.76	0.00152	0.726	19.46	0.00988	0.948	174.9
27.45	21.73	5.43E-4	0.864	15.66	0.0102	0.864	60.01
Ru hcp after 12 h @ 10 mA/cm²							
-8.55	25.42	0.00101	0.908	43.42	0.00834	0.999	1263
5.45	24.15	8.69E-4	0.855	42.16	0.0066	0.968	573.9
15.45	23.84	0.00111	0.814	25.36	0.00809	0.963	241.5
27.45	23.16	0.00111	0.754	26.62	0.00732	0.908	80.62
Ru fcc new film							
-8.55	16.6	5.83E-4	0.943	59.01	0.00496	0.986	726.9
27.45	15.3	9.35E-4	0.762	53.71	0.0045	0.999	69.91
37.45	16.5	4.84E-4	0.869	47.73	0.0051	0.931	42.09
47.45	16.6	4.46E-4	0.868	45.76	0.00694	0.861	24.88
Ru fcc after 12 h @ 10 mA/cm²							
-8.55	16.2	5.46E-4	0.934	139.8	0.00399	1	1147
27.45	15.37	3.62E-4	0.921	92.84	0.00368	0.911	136.6
37.45	14.63	6.16E-4	0.824	36.17	0.00407	0.96	47.91
47.45	14.96	4.48E-4	0.865	54.61	0.00612	0.949	23.99
Comm. Ru/C new film							
-8.55	18.9	4.95E-4	0.99	66.8	0.00462	1	858
27.45	17.45	6.04E-4	0.883	50.03	0.00625	0.963	77.09
37.45	17.56	5.78E-4	0.861	52.12	0.00888	0.988	33.35
47.45	17.66	5.43E-4	0.855	48.36	0.0149	1	14.36
Comm. Ru/C after 12 h @ 10 mA/cm²							
-8.55	17.78	4.16E-4	0.988	207.3	0.00284	1	1453
27.45	14.55	4.62E-4	0.876	154.2	0.00466	1	135
37.45	15.41	3.98E-4	0.903	101.6	0.00631	0.965	67.21
47.45	15.15	3.29E-4	0.913	103.7	0.0119	0.903	32.4

8. Electrochemical active surface area (ECSA) determination and specific activities

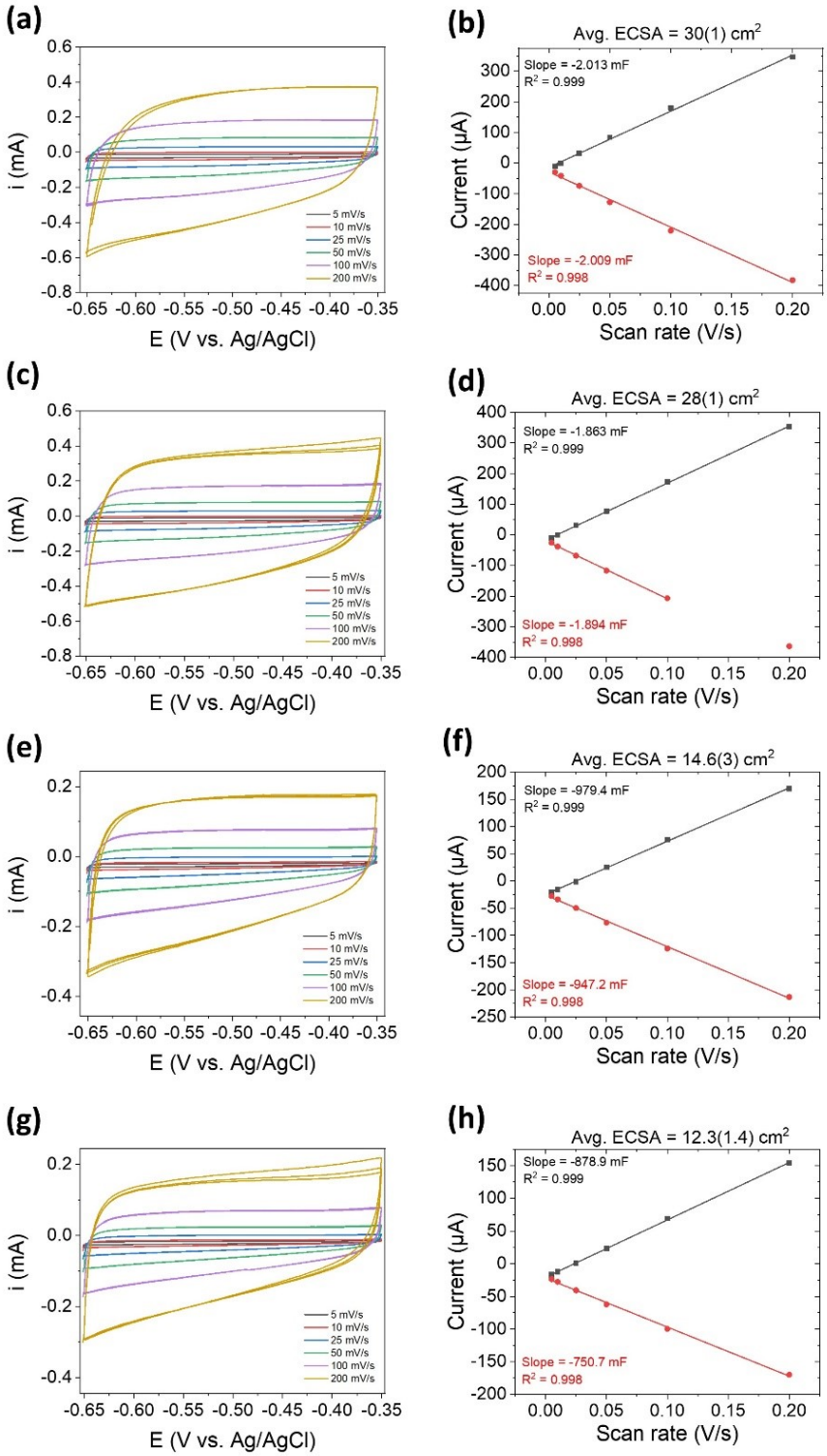

Figure S13. Double-layer capacitance measurements to estimate electrochemically active surface areas (ECSAs) of unsupported homegrown Ru NPs in 1 M NaOH. Cyclic voltammograms were recorded in a non-Faradaic region at scan rates from 5 mV/s to 200 mV/s. The cathodic and anodic charging current are plotted vs scan rate and double layer capacitance is determined from the average value of the linear fits. For hcp Ru NPs before (a,b) and after stability measurements (c,d) and fcc Ru NPs before (e,f) and after stability measurements (g,h).

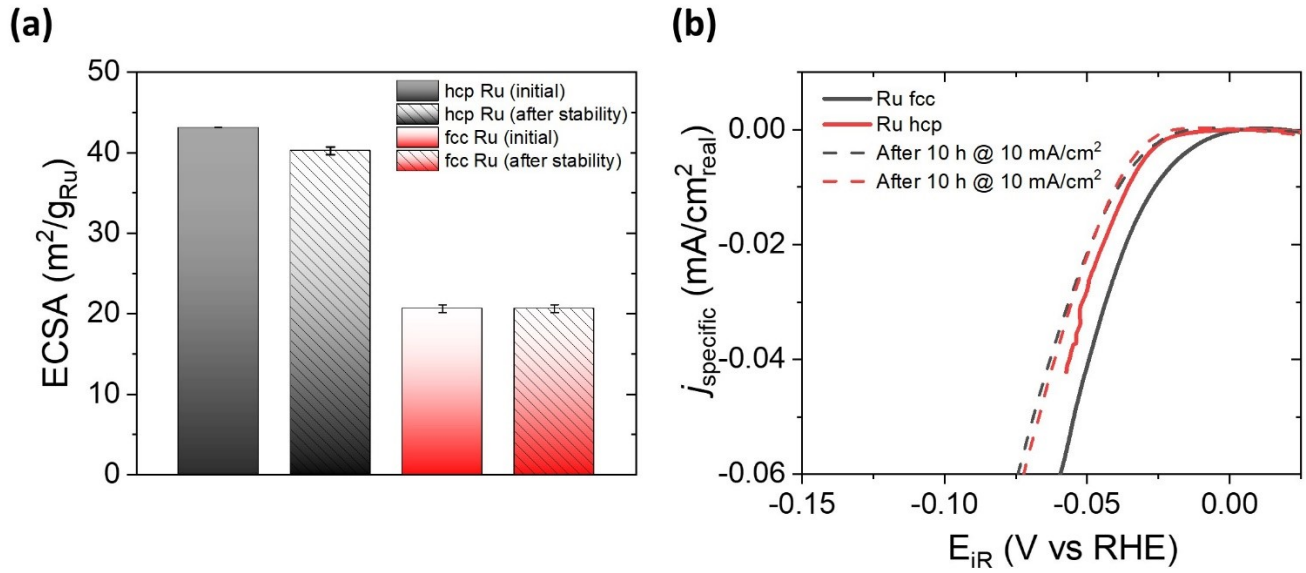

Figure S14. a) Electrochemical active surface area (ECSA). b) Specific activity (normalized by ECSA) measured before and after 12 h stability tests at -10 mA/cm^2.

9. References

[1] a) Rodríguez-Carvajal, J.; Recent advances in magnetic structure determination by neutron powder diffraction. *Physica B* **1993**, *192*, 55-69; b) J. Rodríguez-Carvajal, *Study of Micro-Structural Effects by Powder Diffraction Using the Program FullProf*, Laboratoire Léon Brillouin (CEA-CNRS), CEA/Saclay, 91191 Gif sur Yvette Cedex, FRANCE, **2003**.

[2] Bhowmik, T.; Kundu, M. K.; Barman, S. Growth of One-Dimensional RuO2 Nanowires on g-Carbon Nitride: An Active and Stable Bifunctional Electrocatalyst for Hydrogen and Oxygen Evolution Reactions at All pH Values. *ACS Appl. Mater. Interfaces* **2016**, *8*, 28678-28688.

[3] Mahmood, J.; Li, F.; Jung, S.-M.; Okyay, M. S.; Ahmad, I.; Kim, S.-J.; Park, N.; Jeong, H. Y.; Baek, J.-B. An efficient and pH-universal ruthenium-based catalyst for the hydrogen evolution reaction. *Nat. Nanotech.* **2017**, *12*, 441-446.

[4] Lee, J.; Shah, S. A. S.; Yoo, P. J.; Lim, B. Hydrous RuO2 nanoparticles as highly active electrocatalysts for hydrogen evolution reaction. *Chem. Phys. Lett.* **2017**, *673*, 89-92.

[5] Qiu, T.; Liang, Z.; Guo, W.; Gao, S.; Qu, C.; Tabassum, H.; Zhang, H.; Zhu, B.; Zou, R.; Shao-Horn, Y. Highly exposed ruthenium-based electrocatalysts from bimetallic metal-organic frameworks for overall water splitting *Nano Energy* **2019**, *58*, 1-10.

[6] Creus, J.; Drouet, S.; Suriñach, S.; Lecante, P.; Collière, V.; Poteau, R.; Philippot, K.; García-Antón, J.; Sala, X. Ligand-Capped Ru Nanoparticles as Efficient Electrocatalyst for the Hydrogen Evolution Reaction. *ACS Catal.* **2018**, *8*, 11094-11102.

[7] Wang, Q.; Ming, M.; Niu, S.; Zhang, Y.; Fan, G.; Hu, J. S. Scalable Solid-State Synthesis of Highly Dispersed Uncapped Metal (Rh, Ru, Ir) Nanoparticles for Efficient Hydrogen Evolution. *Adv. Energy Mater.* **2018**, *8*, 1801698

[8] Park, H.-S.; Yang, J.; Cho, M. K.; Lee, Y.; Cho, S.; Yim, S.-D.; Kim, B.-S.; Jang, J. H.; Song, H.-K. RuO2 nanocluster as a 4-in-1 electrocatalyst for hydrogen and oxygen electrochemistry. *Nano Energy* **2019**, *55*, 49-58.

[9] Zheng, Y.; Jiao, Y.; Zhu, Y.; Li, L. H.; Han, Y.; Chen, Y.; Jaroniec, M.; Qiao, S.-Z. High Electrocatalytic Hydrogen Evolution Activity of an Anomalous Ruthenium Catalyst. *J. Am. Chem. Soc.* **2016**, *138*, 16174-16181.

[10] Gao, K.; Wang, Y.; Wang, Z.; Zhu, Z.; Wang, J.; Luo, Z.; Zhang, C.; Huang, X.; Zhang, H.; Huang, W. Ru nanodendrites composed of ultrathin fcc/hcp nanoblades for the hydrogen evolution reaction in alkaline solutions. *Chem. Commun.* **2018**, *54*, 4613-4616.

[11] Bredar, A. R.; Chown, A. L.; Burton, A. R.; Farnum, B. H. Electrochemical Impedance Spectroscopy of Metal Oxide Electrodes for Energy Applications. *ACS Appl. Energy Mater.* **2020**, *3*, 66-98.

[12] Vrubel, H.; Moehl, T.; Grätzel, M.; Hu, X. Revealing and accelerating slow electron transport in amorphous molybdenum sulphide particles for hydrogen evolution reaction. *Chem. Commun.* **2013**, *49*, 8985-8987.